Earth and Planetary Science Letters 349-350 (2012) 53–66

Contents lists available at SciVerse ScienceDirect

Earth and Planetary Science Letters

journal homepage: www.elsevier.com/locate/epsl

Letters

Early Paleogene temperature history of the Southwest Pacific Ocean: Reconciling proxies and models

Christopher J. Hollis [a,*], Kyle W.R. Taylor [b], Luke Handley [b], Richard D. Pancost [b], Matthew Huber [c], John B. Creech [d], Benjamin R. Hines [d], Erica M. Crouch [a], Hugh E.G. Morgans [a], James S. Crampton [a], Samantha Gibbs [e], Paul N. Pearson [f], James C. Zachos [g]

[a] Department of Paleontology, GNS Science, PB 30-368, Lower Hutt 5040, New Zealand
[b] Organic Geochemistry Unit, The Cabot Institute and Bristol Biogeochemistry Research Centre, School of Chemistry, University of Bristol, Bristol BS8 1TS, UK
[c] Earth & Atmospheric Sciences Department and the Purdue Climate Change Research Center, Purdue University, West Lafayette, IN 47907, USA
[d] School of Geography, Environment & Earth Sciences, Victoria University of Wellington, New Zealand
[e] School of Ocean and Earth Sciences, National Oceanography Centre, University of Southampton, Southampton SO14 3ZH, UK
[f] School of Earth & Ocean Sciences, Cardiff University, Cardiff CF10 3AT, UK
[g] Earth & Planetary Sciences, University of California, Santa Cruz, CA 95060, USA

ARTICLE INFO

Article history:
Received 17 November 2011
Received in revised form
22 May 2012
Accepted 14 June 2012
Editor: G. Henderson
Available online 26 July 2012

Keywords:
Paleocene
Eocene
sea temperature
TEX_{86}
oxygen isotopes
magnesium/calcium ratios

ABSTRACT

We present a new multiproxy (TEX_{86}, $\delta^{18}O$ and Mg/Ca), marine temperature history for Canterbury Basin, eastern New Zealand, that extends from middle Paleocene to middle Eocene, including the Paleocene–Eocene thermal maximum (PETM) and early Eocene climatic optimum (EECO). In light of concerns that proxy-based sea surface temperature (SST) estimates are untenably warm for the southwest Pacific during the Eocene, we review the assumptions that underlie the proxies and develop a preliminary paleo-calibration for TEX_{86} that is based on four multiproxy Eocene records that represent an SST range of 15–34 °C. For the southwest Pacific Paleogene, we show that TEX_{86}^{L} exhibits the best fit with the Eocene paleo-calibration. SSTs derived from related proxies (TEX_{86}^{H}, $1/TEX_{86}$) exhibit a systematic warm bias that increases as TEX86 values decrease (a warm bias of 4–7 °C where $TEX_{86} < 0.7$). The TEX_{86}^{L} proxy indicates that southwest Pacific SST increased by ~10 °C from middle Paleocene to early Eocene, with SST maxima of 26–28 °C (tropical) during the PETM and EECO and an SST minimum of 13–16 °C (cool–warm temperate) at the middle/late Paleocene transition (58.7 Ma). The base of the EECO is poorly defined in these records but the top is well-defined in Canterbury Basin by a 2–5 °C decrease in SST and bottom water temperature (BWT) in the latest early Eocene (49.3 Ma); BWT falls from a maximum of 18–20 °C in the EECO to 12–14 °C in the middle Eocene. Overall, cooler temperatures are recorded in the mid-Waipara section, which may reflect a deeper (~500 m water depth) and less neritic depositional setting compared with Hampden and ODP 1172 (~200 m water depth). The high SSTs and BWTs inferred for the PETM and EECO can be reconciled with Eocene coupled climate model results if the proxies are biased towards seasonal maxima and the likely effect of a proto-East Australian Current is taken into account.

1. Introduction

In deciphering the Earth's climate history, we call upon a wide range of geochemical and paleontological proxies for past temperature that vary greatly in reliability and accuracy. To increase confidence in proxy-based temperature estimates, we aim for agreement between different proxies for the same parameter and coherency between proxies for different parameters and between records from different locations. In recent studies of the Paleogene climate history of the southwest Pacific (Burgess et al., 2008; Hollis et al., 2009; Creech et al., 2010), a multiproxy approach has been utilized to identify trends in sea surface and bottom water temperature (SST and BWT), Canterbury Basin, offshore eastern New Zealand, from early to middle Eocene (Fig. 1). The SST trend, based on TEX_{86} and planktic $\delta^{18}O$ and Mg/Ca, agrees well with a single proxy Paleocene–Eocene trend (TEX_{86}) from ODP site 1172, East Tasman Rise, Western Tasman Sea (Bijl et al., 2009, 2010; Sluijs et al., 2011), with a twin proxy record (TEX_{86}, $U^{K'}_{37}$) for the Eocene–Oligocene transition at DSDP Site 277, southwest Campbell Plateau (Liu et al., 2009), and with new TEX_{86}-based SSTs from IODP Site U1356, offshore Wilkes Land, Antarctica (Bijl et al., 2011). The close agreement between these temperature estimates from several high-latitude sites (paleolatitude of 55–65°S) should engender confidence in the veracity of the records. However, the warmest temperatures derived for Canterbury

* Corresponding author.
E-mail address: c.hollis@gns.cri.nz (C.J. Hollis).

0012-821X/$ - see front matter © 2012 Elsevier B.V. All rights reserved.
http://dx.doi.org/10.1016/j.epsl.2012.06.024

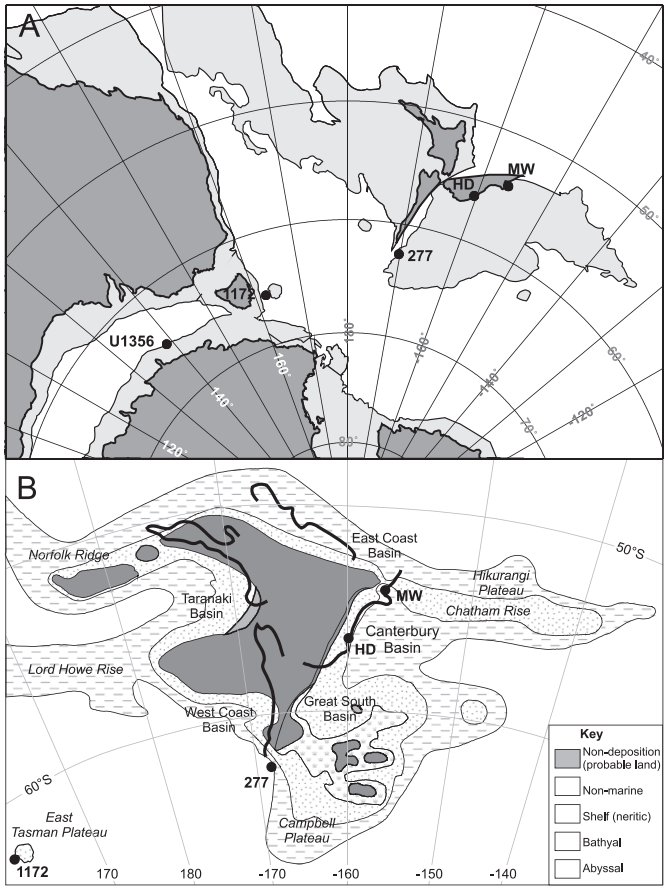

Fig. 1. Location of New Zealand sections, ODP Site 1172 and other localities mentioned in the text on earliest Eocene (A) tectonic reconstruction of southwest Pacific (~54 Ma, modified from Cande and Stock, 2004) and (B) paleogeographic reconstruction of New Zealand region (after King et al., 1999; modified from Hollis et al., 2009). MW=mid-Waipara, HD=Hampden.

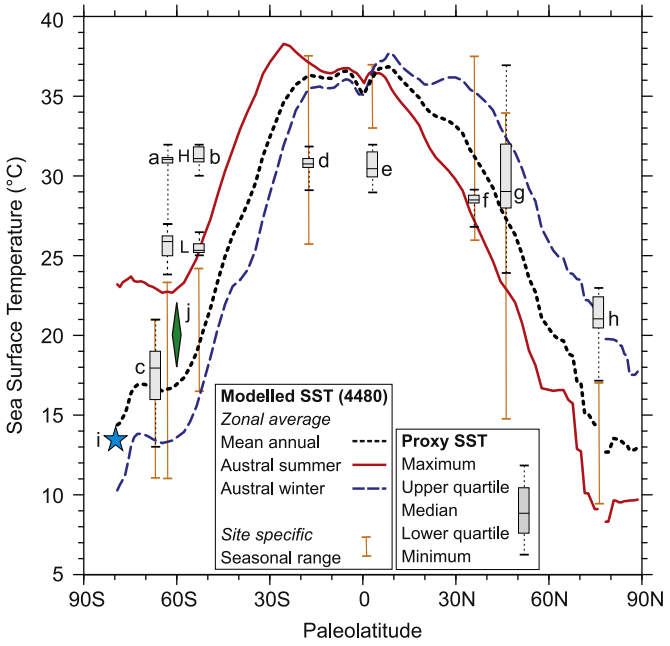

Fig. 2. Comparison sea surface temperature (SST) estimates derived from proxies and an Eocene climate model with 16 × times preindustrial CO_2 (4480 ppmv CO_2-equivalent; NCAR, CCSM3). Proxy SSTs comprise maximum, minimum, median, upper and lower quartile values for the early Eocene climatic optimum (EECO) at (a) ODP Site 1172 (Bijl et al., 2009), (b) mid-Waipara River (Hollis et al., 2009), (c) Seymour Island (Ivany et al., 2008; Douglas et al., 2011), (d) Tanzania (Pearson et al., 2007), (e) ODP Site 865 (Tripati et al., 2003; Kozdon et al., 2011), (f) eastern USA (Keating-Bitonti et al., 2011), (g) Belgian Basin (Vanhove et al., 2011), (h) IODP Site 302-4A, Arctic Basin (Sluijs et al., 2006, 2009). For (a) and (b) the two SST ranges shown are based on the high (H) and low (L) temperature calibrations of Kim et al. (2010). Also shown are (i) median bottom water temperature for the EECO (Cramer et al., 2009) and (j) mean annual air temperature for southeast Australia (Greenwood et al., 2003, 2004). SST estimates for (d) and (g) are derived from TEX86 using the calibration of Liu et al. (2009). SST estimates for (e) and (i) are derived using methodologies discussed in the text. Modeled SST range for each proxy site is also shown. See Supplemental files for data compilation details.

Basin and East Tasman Rise present a major challenge to climate theory and appear to be at odds with other climate proxies, especially paleofloral records (Huber and Caballero, 2011).

During times of peak global warmth in the early Eocene, proxies indicate that high-latitude southwest Pacific SSTs warmed to over 30 °C (Bijl et al., 2009; Hollis et al., 2009; Creech et al., 2010). This either implies a virtual collapse of the zonally averaged equator-to-pole thermal gradient, which cannot be reconciled with the climate dynamics that underpin climate and circulation models (e.g., Huber and Sloan, 2001; Winguth et al., 2010; Lunt et al., 2012), or indicates a peculiarity of the regional climate and circulation. Even in the warmest Eocene climate simulations, the equator-to-pole gradient is >20 °C and mean annual SST for 55–65°S is ~17 °C (Fig. 2). In addition to this proxy-model discrepancy, these SSTs are 10 °C warmer than local mean annual air temperatures (MAAT) derived from leaf fossil studies (18–22 °C; Greenwood et al., 2003, 2004) and are excessively warm in relation to proxy SSTs from other regions, especially the low-latitude Pacific (Tripati et al., 2003; Kozdon et al., 2011) and Indian oceans (Pearson et al., 2007), the Atlantic Ocean (Keating-Bitonti et al., 2011) and the Atlantic sector of the Southern Ocean (Ivany et al., 2008; Douglas et al., 2011). The single exception is the Arctic Ocean where TEX_{86}-based SST is also significantly (~7 °C) warmer than modeled SST (Sluijs et al., 2006, 2009). High-latitude SSTs > 25 °C are also difficult to reconcile with early Eocene deep ocean temperatures maxima of 13–14 °C as indicated by deep sea benthic foraminiferal $\delta^{18}O$ (Zachos et al., 2001, 2008; Cramer et al., 2011).

The uncertainty introduced by these seemingly irreconcilable perspectives is impeding understanding of greenhouse climate dynamics (Kiehl, 2010; Pagani et al., 2011; Valdes, 2011) and the development of a general climate history for the Cenozoic (Hansen et al., 2008; Bertler and Barrett, 2010). In this study we present a TEX_{86}-based temperature record from middle Paleocene to middle Eocene at mid-Waipara River, northern Canterbury Basin, which extends a previous multiproxy study on the Eocene section (Hollis et al., 2009; Creech et al., 2010) and encompasses the Paleocene–Eocene thermal maximum (PETM) as well as the early Eocene climatic optimum (EECO). This record is compared to an early to middle Eocene multiproxy temperature record at Hampden Beach, southern Canterbury Basin (Burgess et al., 2008; Morgans, 2009) and the middle Paleocene to middle Eocene TEX_{86}-based SST record from ODP Site 1172, East Tasman Plateau (Bijl et al., 2009, 2010; Sluijs et al., 2011). In an effort to reconcile these proxy records with other proxy-based and modeled temperature reconstructions, we review the premises that underpin the three primary proxies for SST: $\delta^{18}O$, Mg/Ca and TEX_{86}. We conclude by comparing proxy-based marine temperatures with modeled temperatures derived from a fully coupled general circulation model with Eocene boundary conditions.

2. Material and methods

This study is based on sedimentary rock samples collected from the Paleocene–Eocene succession exposed along the middle

branch of the Waipara River (mid-Waipara), northern onshore Canterbury Basin, and the Eocene succession exposed at Hampden Beach, southern onshore Canterbury Basin (Fig. 1). At mid-Waipara, a series of low-dipping sections has been logged, sampled and integrated into a single composite section (Morgans et al., 2005). This study is based on two sub-sections, referred to as Columns 2 and 6 (Fig. 3). Column 2 extends from upper Loburn Formation to basal Ashley Mudstone (lower Paleocene to lowermost Eocene). Column 6 consists of lower to middle Eocene Ashley Mudstone. New data from spot samples collected through the poorly exposed lower part of Column 6 are combined with previously reported data (Hollis et al., 2009; Creech et al., 2010). From a total of 66 samples, 46 have been analyzed for TEX_{86}, including 26 new samples from the Paleocene and lowermost Eocene interval (Column 2 and lower Column 6); 44 samples have been analyzed for total organic carbon (TOC) and bulk organic $\delta^{13}C$ ($\delta^{13}C_{TOC}$), including 23 new samples from the Paleocene, and the elemental composition of these 23 samples has also been determined by X-ray fluorescence (see Supplemental files). Foraminiferal assemblages in the Paleocene–lowermost Eocene (Teurian–Waipawan) interval are too sparse or poorly preserved for stable isotope or Mg/Ca analysis of foraminifera. Paleocene carbonate content is too low for bulk carbonate stable isotope analysis. Eocene foraminiferal $\delta^{18}O$ and Mg/Ca data are derived from Hollis et al. (2009) and Creech et al. (2010).

At Hampden Beach, a low-dipping coastal section has been logged and sampled for a study of foraminiferal biostratigraphy and paleoecology (Morgans, 2009). Selected samples and foraminiferal assemblages from the lower to middle Eocene Kurinui Formation are incorporated into this study to compare paleotemperature trends between the northern and southern parts of Canterbury Basin (Fig. 4). New analyses undertaken include an Mg/Ca study of benthic and planktic foraminifera in 15 samples

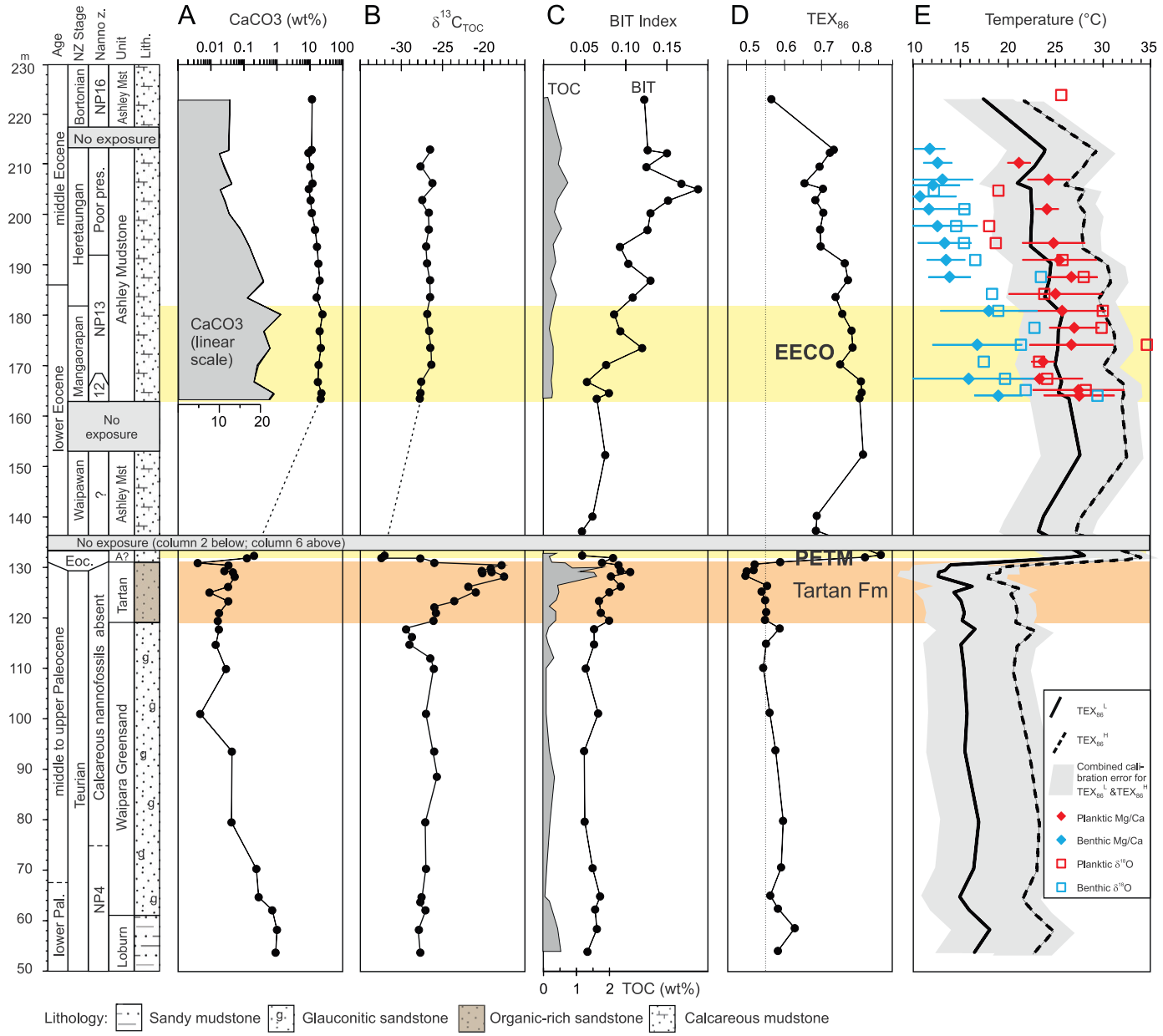

Fig. 3. Stratigraphy and geochemical trends in the mid-Waipara section, including (A) $CaCO_3$ concentration, (B) $\delta^{13}C$ of total organic carbon (TOC), (C) BIT index and TOC, (D) TEX_{86}, and (E) estimated sea surface and bottom water temperature. In (E) the combined calibration error for TEX_{86} incorporates ± 2.5 °C and ± 4 °C for TEX_{86}^{H} and TEX_{86}^{L}, respectively (Kim et al., 2010); error bars for Mg/Ca are 95% confidence intervals on the range of temperatures recorded from multiple measurements of multiple specimens in each sample or the calibration error of ± 1.2 °C (Anand et al., 2003), depending on which value is larger; calibration errors are not shown for $\delta^{18}O$ (± 2.15 °C; Erez and Luz, 1983).

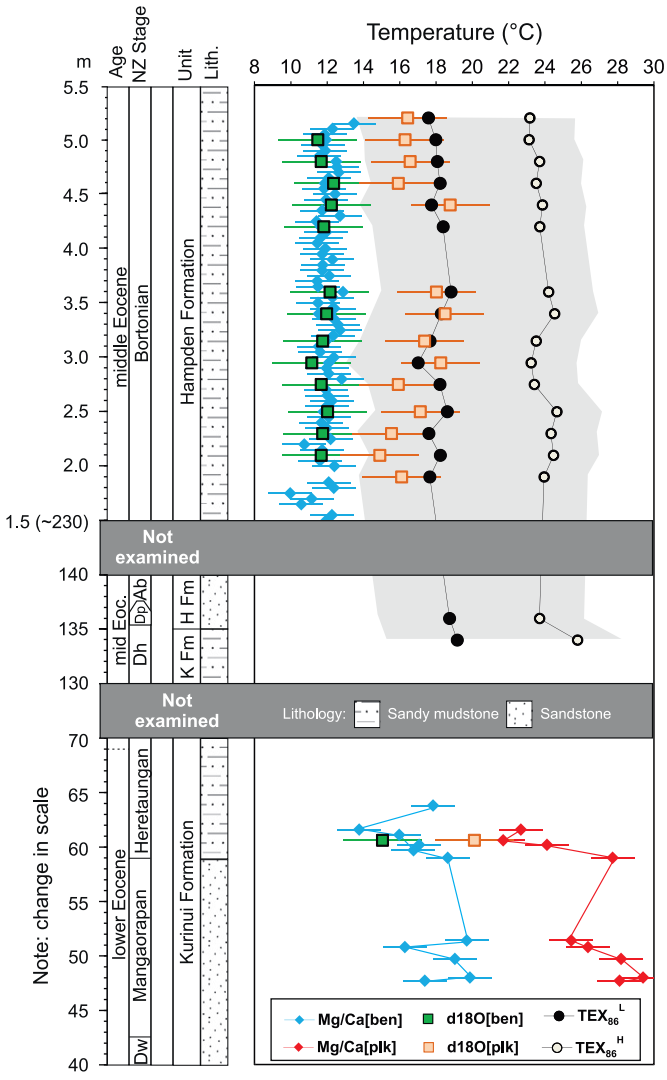

Fig. 4. Stratigraphy and marine temperature estimates for lower to middle Eocene, Hampden section. Error ranges as in Fig. 3, except that the calibration error for $\delta^{18}O$ is also shown (± 2.15 °C). Abbreviations for New Zealand stages: Dw=Waipawan, Dh=Heretaungan; Dp=Porangan; Ab=Bortonian.

that span the early–middle Eocene transition (late Mangaorapan to early Heretaungan, 51 – 48 Ma), TEX_{86} analysis of two samples near the early/middle Eocene boundary and detailed stable isotope study of a single early Eocene foraminiferal assemblage (see Supplemental files). These analyses complement a high-resolution multiproxy study of a 5 m-thick interval within the middle Eocene Hampden Formation (Burgess et al., 2008).

Age control is based on dinoflagellate cyst, calcareous nannofossil and foraminiferal biostratigraphy for the mid-Waipara section (see Supplemental files) and on foraminiferal biostratigraphy for the Hampden section (Morgans, 2009). Bioevents and New Zealand stages are calibrated to the 2004 Geological Timescale (Gradstein et al., 2004; Ogg et al., 2008; Hollis et al., 2010). Benthic foraminifera indicate upper bathyal (~500 m) paleodepth for the mid-Waipara section in the early Eocene and a shallower outermost shelf (~200 m) setting for coeval strata at Hampden (Hollis et al., 2009; Morgans, 2009).

3. Paleotemperature calibrations

In order to examine possible causes for anomalously high proxy-based SST estimates, we carefully considered the analytical approach for each of the proxies used in this study. For oxygen isotopes, paleotemperature is calculated using the equation of Kim and O'Neil (1997) as expressed in Bemis et al. (1998) for both benthic and planktic foraminifera and bulk carbonate. Bemis et al. (1998) show that this equation provides a better fit to core-top data for the epifaunal benthic genus *Cibicidoides* than the alternative equations commonly used for benthic foraminifera (i.e., Shackleton, 1974; Erez and Luz, 1983). The equation yields slightly cooler temperatures (up to ~1 °C) than those derived from the Erez and Luz (1983) equation but are more in line with the revised planktic equations developed by Bemis et al. (1998). For these reasons, we use this equation for both planktic and benthic foraminifera. In keeping with prior work (Zachos et al., 2008), we make the assumption that ice sheets were absent from early Paleogene landmasses. We use a $\delta^{18}O_{SW}$ value of −1.30‰ (vPDB) for Canterbury Basin. This incorporates a vSMOW to vPDB correction of −0.27‰ (Bemis et al., 1998), an ice volume value of −0.96‰ (Zachos et al., 1994) and a latitudinal correction for $\delta^{18}O_{SW}$ of −0.07‰ for 55°S (Zachos et al., 1994), which is based on modern latitudinal gradients. For other sites referred to in this study, we also apply a latitudinal correction of Zachos et al. (1994). Although modeling approaches to derive $\delta^{18}O_{SW}$ for the Eocene have potential (Bice et al., 2000; Huber et al., 2003; Tindall et al., 2010; Roberts et al., 2011), they are not used here because large discrepancies are evident between different approaches. For example, modeled $\delta^{18}O_{SW}$ values for the Canterbury Basin region range from −1.63 (Tindall et al., 2010) to −0.25 (Roberts et al., 2011), which translates to a temperature difference of ~7 °C. We apply no correction for localized potential salinity, pH or carbonate ion effects.

For foraminiferal Mg/Ca ratios, we use the equations of Lear et al. (2000, 2002) and Anand et al. (2003) as described by Creech et al. (2010). We have adopted a Mg/Ca ratio of 4 mmol/mol for early and middle Eocene seawater (Mg/Ca_{SW}) based on comparative studies of foraminiferal Mg/Ca ratios and $\delta^{18}O$ values (Lear et al., 2002; Sexton et al., 2006). These studies suggest a range of 3–5 mmol/mol for the early Eocene Mg/Ca_{SW} with higher values more in line with temperatures derived from $\delta^{18}O$ for ice-free conditions (Sexton et al., 2006). We recognize that this foraminifera-based approach to estimating Eocene Mg/Ca_{SW} yields values that are lower than those derived from other methods (e.g. Farkaš et al., 2007; Coggon et al., 2010, 2011) and see promise in current research to reconcile these different approaches through consideration of the effects of carbonate saturation state (Lear et al., 2010) and Mg partitioning (Hasiuk and Lohmann, 2010) and scrutiny of existing foraminiferal calibrations (Broecker and Yu, 2011; Cramer et al., 2011). An Mg/Ca_{SW} value of 4 mmol/mol yields temperatures that are ~2 °C cooler than those reported previously (Hollis et al., 2009; Creech et al., 2010) which were based on a value of 3.35 mmol/mol.

For GDGT-based temperature proxies, there are currently three commonly utilized equations: $1/TEX_{86}$ (Liu et al., 2009), TEX_{86}^{H} and TEX_{86}^{L} (Kim et al., 2010). TEX_{86}^{H} comprises the same combination of GDGTs as in the original TEX_{86} relationship (Schouten et al., 2002; Kim et al., 2008) but the calibration with SSTs is based mainly on a low- to mid-latitude core-top data set and it is recommended for SST records above 15 °C. It has a calibration error of ±2.5 °C. TEX_{86}^{L} comprises a combination of GDGTs that differs from TEX_{86}^{H} and all other TEX_{86} equations and does not employ the crenarchaeol isomer. It is calibrated to a global dataset and has a calibration error of ±4 °C. Kim et al. (2010) recommend that TEX_{86}^{L} is applied to paleo-SST records that range below 15 °C. The calibration of Liu et al. (2009) as revised by Kim et al. (2010), utilizes the same GDGT combination as TEX_{86}^{H} but is based on a reciprocal rather than log relationship. It has a calibration error of ±5.4 °C. Kim et al. (2010) showed that SSTs

derived from $1/TEX_{86}$ typically fall between those derived from TEX_{86}^{L} and TEX_{86}^{H}.

GDGT-based SST can be biased by the input of terrestrial GDGTs. This bias is thought to be minimal when the branched vs. isoprenoid (BIT) index is lower than 0.3 (Weijers et al., 2006). The BIT index reflects the relative contribution of soil-derived (non-isoprenoidal) and marine GDGTs (Hopmans et al., 2004).

4. Results

4.1. Stratigraphy of mid-Waipara section

The mid-Waipara section (Columns 2 and 6) extends from lower Paleocene (lower Teurian, ~63 Ma) to middle Eocene (Bortonian, ~40 Ma) (Fig. 3). A sharp contact separates upper Paleocene strata (Waipara Greensand) from the calcareous mudstone at the top of the Column 2, which is identified as basal Eocene (lower Waipawan, 55.8 Ma). Low carbonate content relative to typical Ashley Mudstone suggests that this unit is basal Ashley Mudstone. In Column 6, planktic foraminifera identify a lower Eocene (Waipawan, 55.8–53.3 Ma) interval of Ashley Mudstone below the lower Eocene to middle Eocene (Mangaorapan–Bortonian, 53.3–40 Ma) interval that formed the basis of our previous studies (Hollis et al., 2009; Creech et al., 2010). The latter interval includes a well exposed 50-m thick section that extends from lower Mangaorapan to upper Heretaungan (52–45.4 Ma) and spans the Mangaorapan/Heretaungan stage boundary (49.3 Ma). Strata spanning the Waipawan/Mangaorapan, Heretaungan/Porangan and Porangan/Bortonian stage boundaries are covered by Quaternary river gravels. It is possible that the entire Porangan stage (45.3–42.8 Ma) is missing at this locality.

Carbonate content serves to identify five deposition phases in this section (Fig. 3A): two intervals that are slightly calcareous (0.1–1% $CaCO_3$; lower Paleocene, basal Eocene), an upper Paleocene interval that is non-calcareous ($<0.1\%$ $CaCO_3$), a lower Eocene interval that is highly calcareous ($>15\%$ $CaCO_3$), and the moderately calcareous middle Eocene (10–14% $CaCO_3$). Carbonate content is too low to yield a robust carbonate $\delta^{13}C$ record for the entire section. However, bulk organic $\delta^{13}C$ ($\delta^{13}C_{TOC}$) helps to refine the stratigraphy (Fig. 3B). Through much of the section, $\delta^{13}C_{TOC}$ is remarkably stable at $-27‰$, a value that is typical for marine organic matter in these sediments from Late Cretaceous to Eocene (Hollis et al., 2003, 2005). In the upper Paleocene, a 7–9‰ positive excursion that spans 10 m is associated with comparatively high TOC of 0.5–1.6 wt%. This is the geochemical signature of a marine source rock unit that is widespread in the late Paleocene, especially eastern New Zealand (Killops et al., 2000; Hollis et al., 2005). Although the unit is more widely known as the Waipawa Formation, we follow Schiøler et al. (2010) and assign this interval to the Tartan Formation, a facies-equivalent to the Waipawa Formation that occurs in the Great South and Canterbury Basins.

Above the Tartan Formation, and separated by an unconformity, a ~5‰ negative excursion in $\delta^{13}C_{TOC}$ (from background values of $\sim -27‰$ to $-32‰$) serves to identify the PETM within the basal Ashley Mudstone. Although the P–E transition is poorly exposed, the magnitude of this excursion is close to the average of 4‰ recorded for the PETM in marine organic matter (McInerney and Wing, 2011). Identification of the PETM is supported by four dinoflagellate criteria: (1) the presence of *Manumiella rotunda* implies that the unit is no younger than early Waipawan (~55 Ma; Cooper, 2004; Hollis et al. 2010), (2) the interval contains *Apectodinium*, albeit in low abundance; *Apectodinium* first occurs slightly below the P/E boundary in New Zealand and typically has an acme within the PETM (Crouch et al., 2001), (3) the interval contains *Hystrichokolpoma*, a genus that first occurs in the PETM at Tawanui and the Kumara drillhole (Crouch et al., 2001; Handley et al., 2011), and (4) the basal sample contains an influx of *Glaphyrocysta*, which also has an abundance peak at the base of the PETM at Tawanui, North Island, New Zealand (Crouch and Brinkhuis, 2005) and at ODP Site 1172 (Sluijs et al., 2011).

4.2. Paleotemperatures in mid-Waipara and Hampden sections

Low BIT indices in the mid-Waipara (Fig. 3C) and Hampden Beach sections (<0.27; Burgess et al., 2008) suggest minimal influence of soil lipids on the GDGT-based SST proxies. At mid-Waipara, TEX_{86} values indicate a distinct shift from relatively cool conditions in the Paleocene to very warm conditions in the PETM and EECO (Fig. 3D). Intermediate values are recorded for the post-PETM earliest Eocene and middle Eocene. We use TEX_{86}^{H} and TEX_{86}^{L} to delimit the likely temperature range (Fig. 3E), while noting calibration errors of ± 2.5 °C and ± 4 °C, respectively, for these two proxies (Kim et al., 2010). Temperature estimates are also shown for previously reported foraminiferal Mg/Ca ratios and $\delta^{18}O$ values for the Eocene (Hollis et al., 2009; Creech et al., 2010) using the equations and correction factors outlined above. The three SST proxies exhibit similar trends, and SSTs derived from planktic foraminiferal Mg/Ca and TEX_{86}^{L}agree. BWTs derived from benthic foraminiferal Mg/Ca and $\delta^{18}O$ also are in good agreement although there is greater variation in both planktic and benthic $\delta^{18}O$.

The wide scatter in $\delta^{18}O$ values suggests that diagenesis of foraminifera has had two contrasting effects. Anomalously cool temperatures in three planktic foraminiferal $\delta^{18}O$ data points in the early–middle Eocene appear to reflect the local influence of corrosive deep water during an episode of climatic cooling following the EECO (Hollis et al., 2009). Pearson et al. (2007) argue that early diagenesis and absorption of isotopically heavy carbonate at the seafloor increased through the Eocene as bottom waters cooled and became more corrosive. Similarly anomalous cool temperatures are evident in planktic $\delta^{18}O$ in the same time interval at DSDP Site 277 (Shackleton and Kennett, 1975; Hollis et al., 2009). Conversely, anomalously warm temperatures are evident for five planktic samples and two benthic samples. The presence of secondary calcite overgrowths on foraminifer tests suggests that the strongly negative $\delta^{18}O$ signature may be the result of a late phase of diagenetic alteration under the influence of meteoric pore waters (Zachos and Arthur, 1986; Hollis et al., 2003). The implication of finding evidence for both these effects at mid-Waipara is that $\delta^{18}O$ values that do not appear anomalous may actually be recording the effects of both the early and late phases of diagenesis. For this reason, we consider all planktic $\delta^{18}O$ values from this section unreliable. In contrast, the temperatures derived from benthic $\delta^{18}O$ are considered reliable, apart from the two samples that appear to have been affected by late phase diagenesis.

Agreement between SSTs derived from planktic Mg/Ca and TEX_{86}^{L} in the Eocene provides some confidence in the SST estimates derived from TEX_{86}^{L} for the Paleocene. Thus, we infer that SST was relatively cool in the Paleocene (~16 °C) with minimum SST in the upper Tartan Formation (~13 °C). SST was much warmer in the Eocene (~23 °C), with peak temperatures in the PETM and EECO of ~26–27 °C. Benthic Mg/Ca and $\delta^{18}O$ indicate BWT decreased by ~4 °C across the Mangaorapan/Heretaungan boundary (49.3 Ma), from 16–18 °C in the early Eocene to 11–14 °C in the middle Eocene. A significant increase in the SST–BWT temperature gradient is also observed at this boundary: from 8 °C in the early Eocene to 12 °C in the middle Eocene. As the EECO is generally defined by the benthic $\delta^{18}O$ record (Zachos et al., 2008), we use the BWT record in this section to correlate the EECO with the Mangaorapan stage (53.3–49.3 Ma). As noted

previously (Hollis et al., 2009; Creech et al., 2010), SST cooled ~1 m.y. later in this section (~48 Ma).

In the Hampden section, foraminiferal Mg/Ca ratios indicate that the Mangaorapan (Fig. 4) may have been slightly warmer than at mid-Waipara, with average SSTs and BWTs of 28 °C and 18 °C, respectively. This may reflect the shallower depositional setting (Morgans, 2009). However, the Mangaorapan/Heretaungan boundary at Hampden is associated with 5–6 °C of cooling in both SST and BWT. Apart from the warm BWT in a single sample, this cooling is consistent with the relatively cool, high-resolution, multiproxy temperature record from the Bortonian Hampden Formation (Burgess et al., 2008).

There is close agreement between BWTs derived from benthic $\delta^{18}O$ and Mg/Ca, which are very stable at 12 °C, and between SSTs derived from planktic foraminiferal $\delta^{18}O$ and TEX_{86}^{L}, which range from 16 °C to 18 °C (Fig. 4). TEX_{86}^{H}-based SSTs are higher and very similar to the SSTs reported by Burgess et al. (2008), which were based on the TEX_{86} calibration of Kim et al. (2008). Burgess et al. (2008) suggested that the 5–7 °C offset from the $\delta^{18}O$-based temperatures could be explained by the inferred biology of the planktic foraminifer measured: *Globigerinatheka index*. This species is thought to have developed thick calcitic overgrowths at depth during gametogenesis (Boersma et al., 1987; Pearson et al., 2006). However, this phenomenon appears to be confined to low latitudes and typically does not cause an offset from SST of > 2 °C (Boersma et al., 1987).

5. Discussion

5.1. A comparison of GDGT proxies to other SST proxies in the Paleogene

In order to have confidence in using GDGT-based SST proxies such as TEX_{86} in ancient sediments, it is useful to consider the general principle that underpins these proxies. The TEX_{86} proxy was derived from observations of ocean surface sediments and laboratory experimentation that identified a clear relationship between the number of cyclopentane moieties in membrane lipids derived from marine Thaumarchaeota and growth temperature (Schouten et al., 2002). There is little dispute over this general physiological relationship (Gliozzi et al., 1983; Wuchter et al., 2006; Schouten et al., 2007). The debate centers on the applicability of this modern calibration to temperature reconstruction in deep time, especially the early Cenozoic and Mesozoic. One way to test the suitability of a calibration for the Paleogene is to assemble the Paleogene equivalent of a core-top data set (Fig. 5). We have taken four Eocene records in which a representative range of TEX_{86} values from 0.60 to 0.93 can be tied to SST estimates derived from $\delta^{18}O$ values or Mg/Ca ratios in well-preserved mixed-layer planktic foraminifera, i.e. Wilson Lake, New Jersey (Zachos et al., 2006), Tanzania (Pearson et al., 2007), Hampden (Burgess et al., 2008) and mid-Waipara (Hollis et al., 2009; Creech et al. 2010). In each case, we have recalculated $\delta^{18}O$-derived temperatures as outlined above (see Supplemental files).

A strong correlation is observed between TEX_{86} values and SSTs derived from inorganic proxies at these four sites (Fig. 5A). The best fit trend-line is a logarithmic regression ($r^2=0.87$, $n=42$, $p<0.001$). The 95% prediction band can be used to interrogate the SST estimates derived from the three main GDGT calibrations (Fig. 5B). For southwest Pacific Paleogene GDGT records (combined data from mid-Waipara, Hampden and ODP Site 1172), SST estimates derived from $1/TEX_{86}$ and TEX_{86}^{H} overestimate temperatures by an increasing amount as TEX_{86} values decrease, with offsets exceeding 5 °C where $TEX_{86}<0.70$. TEX_{86}^{L}-derived SSTs mainly lie within the 95% prediction and exhibit a trend that is slightly shallower than the regression, resulting in slightly lower SSTs where $TEX_{86}>0.75$ and higher SSTs for lower TEX_{86} values. The scatter in these SST estimates is because TEX_{86} is based on a GDGT relationship that differs from that used for TEX_{86}. A similar pattern emerges if we perform the regression using the GDGT relationship that underlies TEX_{86}^{L} (GDGT-1 index; Fig. 5C). Here, the best fit trend-line is also a logarithmic regression. There is wide scatter in the Tanzanian data and the overall correlation to SST is weaker ($r^2=0.71$, $n=41$, $p<0.001$) than with TEX_{86}. Southwest Pacific SST estimates derived from $1/TEX_{86}$ and TEX_{86}^{H} generally lie within the 95% prediction band but exhibit wide scatter and most values lie above the trend-line, especially where GDGT-1 < 0.45. However, TEX_{86}^{L} derived-SSTs fall on a curve that lies within the 95% confidence band.

The observed correlations indicate that the strong relationship between GDGT distributions and SST also existed during the Paleogene. The regression equation identified for TEX_{86} provides a useful way to test established GDGT calibrations against other temperature proxies. We define this paleo-SST regression as $pTEX_{86}$, where

$$SST = 39.036 \times \ln(TEX_{86}) + 36.455$$

When compared to $pTEX_{86}$, the $1/TEX_{86}$ and TEX_{86}^{H} calibrations yield southwest Pacific SSTs that are anomalously high, with lower offsets at higher temperatures (Fig. 5A). Although not shown, the same relationship is evident with all earlier calibrations based on TEX_{86}. This is not the case for TEX_{86}^{L} which yields temperatures that generally fall within the prediction range of the $pTEX_{86}$ regression and generates a correlation that deviates only slightly from the trend-line in the GDGT-1 regression. This indicates that TEX_{86}^{L} is the GDGT proxy most consistent with other proxies and the most appropriate for estimating SST in the southwest Pacific Paleogene. GDGT data from other regions may be plotted against this regression curve as a way of selecting optimal GDGT proxies (see Supplemental files). For the low latitude records from Wilson Lake and Tanzania (Zachos et al., 2006; Pearson et al., 2007), where TEX_{86} values range higher than 0.85, all GDGT proxies lie within the 95% prediction band but the best fit is with $1/TEX_{86}$.

5.2. Systematic offsets between GDGT values and SSTs derived from inorganic proxies

Systematic offsets are observed between GDGT values (TEX_{86} and GDGT-1) and SSTs derived from inorganic proxies at each of the four localities included in our reference dataset. For mid-Waipara, Wilson Lake and Tanzania, the offset reflects wide variation in GDGT values associated with a narrow range of SST values. The cause of this variation is uncertain but it may be related to seasonal or oceanographic variability in GDGT production (e.g., Huguet et al., 2007). For Hampden, however, the offset records wide variation in SST associated with a more narrow range of GDGT values. This relationship was noted by Burgess et al. (2008) when describing the cyclical variation in temperature estimates in the Hampden section. They observed that the cyclical temperature range derived from $\delta^{18}O$ was almost twice the TEX_{86}-based range and suggested that variation in planktic foraminifer $\delta^{18}O$ might have been amplified by cyclical changes in salinity or ocean thermal structure. However, a small but significant contribution from global ice volume changes cannot be discounted (Burgess et al., 2008). This would have implications for the SSTs calculated for the Hampden section, which impacts on the $pTEX_{86}$ relationship we have derived. This observation highlights that SST estimates, especially at the lower temperature range, will continue to evolve not only with new interpretations of GDGT data, but also new interpretations of inorganic proxies.

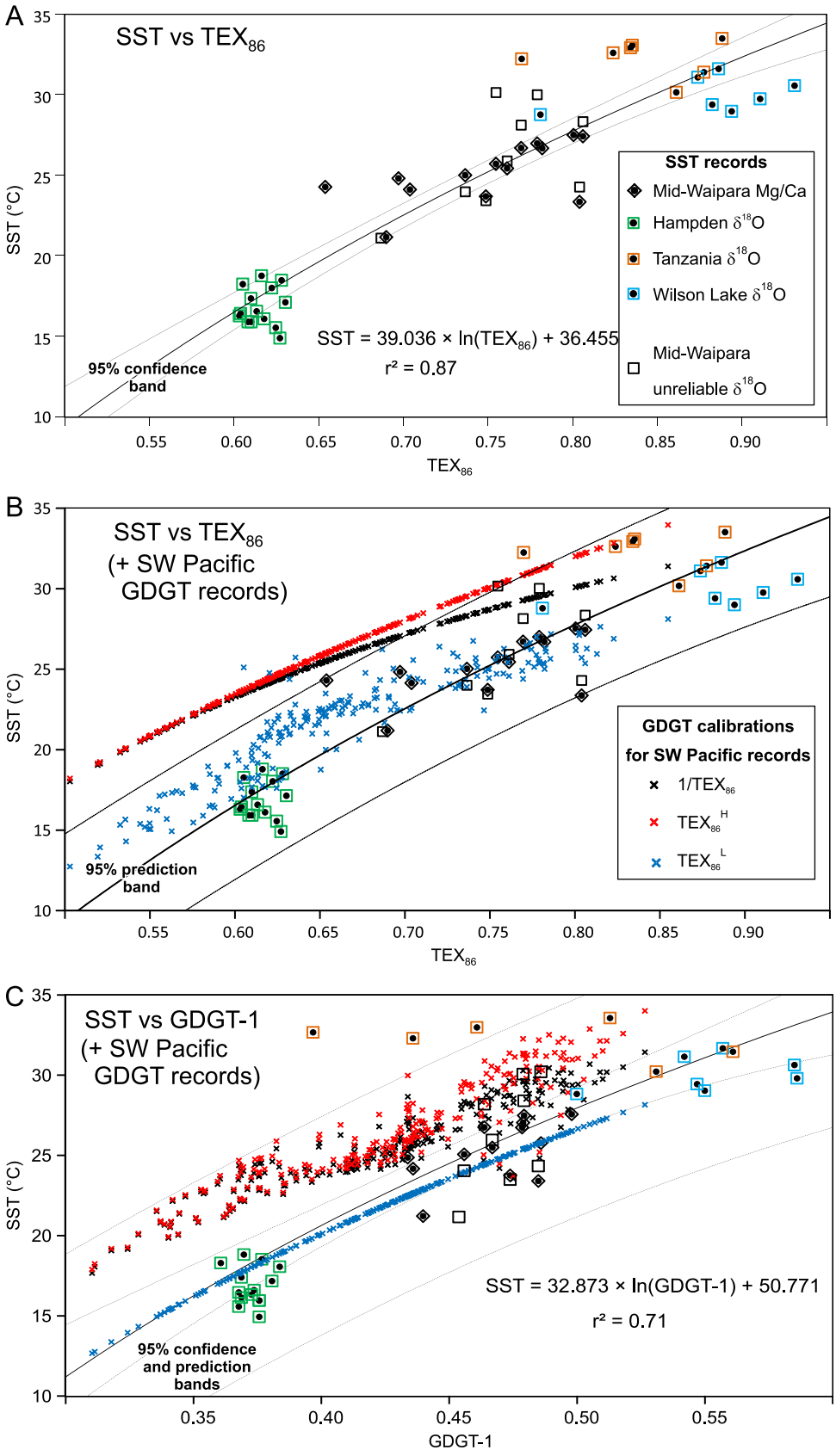

Fig. 5. Sea surface temperatures (SSTs) derived from inorganic proxies compared to TEX_{86} values (A, B) and GDGT-1 values (C). In (5A) TEX_{86} is compared to SSTs derived from $\delta^{18}O$ in well-preserved planktonic foraminifera from Wilson Lake, New Jersey (Zachos et al., 2006), Tanzania (Pearson et al., 2007) and Hampden (Burgess et al., 2008) and from Mg/Ca ratios in well-preserved foraminifera from mid-Waipara (Creech et al., 2010). Unreliable $\delta^{18}O$ records from mid-Waipara are also shown. The best fit to the data is a logarithmic regression. The 95% confidence band shows the expected value of mean SST for any given TEX_{86} value. In (B) SSTs derived from TEX_{86}^{L}, TEX_{86}^{H} and $1/TEX_{86}$ for Canterbury Basin and ODP Site 1172 are plotted on the paleo-SST/TEX_{86} regression. The 95% prediction band shows the range within which we expect SSTs estimates derived from TEX_{86} to be located. In (C) SSTs derived from TEX_{86}^{L}, TEX_{86}^{H} and $1/TEX_{86}$ for Canterbury Basin and ODP Site 1172 are plotted on the best-fit logarithmic regression that compares paleo-SST with the GDGT-1 index, the index that underlies the TEX_{86}^{L} proxy. The 95% prediction band shows the range within which we expect SSTs estimates derived from GDGT-1 to be located.

5.3. Why are SSTs derived from TEX_{86}^{H} and $1/TEX_{86}$ too high?

Following the recommendations of Kim et al. (2010), TEX_{86}^{H} should be the most appropriate GDGT-based SST proxy for these southwest Pacific records because previous studies suggested a SST range of 20–30 °C from the Paleocene to middle Eocene (Bijl et al., 2009; Hollis et al., 2009). However, our analysis shows that SSTs derived from TEX_{86}^{H} and $1/TEX_{86}$ are higher than those derived from inorganic proxies, whereas TEX_{86}^{L} yields SSTs that are broadly consistent with them. Regardless of comparisons with other proxies, the offset between these GDGT-based SSTs is surprising because all three proxies yield similar temperatures for SSTs > 15 °C in the modern dataset. To further add to the confusion, a study of modern core-top GDGT data from the southwest Pacific (Ho et al., 2011) also shows a negligible offset between SSTs derived from TEX_{86}^{H} and TEX_{86}^{L} but these SSTs are consistently 3–8 °C higher than instrumental SST measurements for this region, which has a mean annual SST range of 10–20 °C. Previous studies (Liu et al., 2009; Kim et al. 2010) highlighted the observation that there is large scatter in TEX_{86}-derived SSTs values in the low temperature range (< 5 °C), and this was attributed to different physiological relationships. However, this lower temperature range corresponds with higher latitudes (> 60°N, > 50°S) and it is possible that factors other than SST may have a significant influence on GDGT distributions in those oceanographic settings. Although TEX_{86}^{H} and TEX_{86}^{L} have been presented as high- and low-temperature GDGT proxies for SST (Kim et al., 2010), it may be more appropriate to treat them as low- and high-latitude proxies simply because a weak correlation with high-latitude SST can be observed for TEX_{86}^{L} but not for TEX_{86}^{H}.

It is also possible that the Paleogene SST–GDGT relationship is not exactly the same as the present-day relationship. Whilst we have demonstrated that there is a general agreement between TEX_{86} and inorganic proxies for SST, it is possible that Paleogene oceans were inhabited by different archaeal assemblages from those that dominate today. Unusual GDGT distributions in mesocosm studies (e.g., Wuchter et al., 2006) suggest that the assemblage preserved in sediments reflects a combination of physiological and ecological signatures. Ancient greenhouse oceans were characterized by elevated temperatures, associated differences in water column structure, but also elevated CO_2 (Pearson and Palmer, 2000; Beerling and Royer, 2011), lower pH (Pearson and Palmer, 2000), and possibly lower O_2 (Kurtz et al., 2003). We cannot preclude that such conditions resulted in a shift in the distribution of thaumarchaeotal species, or that new species or new adaptations arose as the global oceans cooled.

5.4. A revised sea temperature history for the southwest Pacific Paleogene

Based on the previous discussion, we argue that TEX_{86}^{L} is the most accurate GDGT-based approach to reconstruct trends in paleotemperature in the Canterbury Basin and the East Tasman Plateau, and potentially in other higher latitude regions. For late Paleocene to middle Eocene records from the southwest Pacific (Fig. 6), SST estimates derived from TEX_{86}^{L} are in agreement with those derived from $pTEX_{86}$. Particularly close agreement is observed between TEX_{86}^{L} and $pTEX_{86}$ during the early Eocene, especially in the EECO. Whereas there is generally good agreement between TEX_{86}^{L} and $pTEX_{86}$ throughout the Paleocene–Eocene interval at mid-Waipara, TEX_{86}^{L}-based SSTs are 2–3 °C higher than $pTEX_{86}$ in the late Paleocene and middle Eocene at ODP Site 1172. As noted earlier, this offset develops where SSTs fall below 22–24 °C, but it appears to be a particular feature of Site 1172 although $pTEX_{86}$ values still lie within the calibration error of TEX_{86}^{L}. Reasons for this offset are unclear.

A warm temperate climate (SST of ~16–19 °C) prevailed through much of the Paleocene (62–56 Ma) in the southwest Pacific (55–65°S), with short-lived cooling to cool temperate conditions (SST, 13–16 °C) occurring at ~58.7 Ma (Table 1). A pronounced warming trend between 58 and 53 Ma saw SST increase by 10 °C, reaching a maximum of ~26–28 °C in the EECO. A short-lived 5 °C warming at the PETM was superimposed upon this trend, but PETM temperatures may not have exceeded maximum temperatures within the EECO. The termination of the EECO is associated with pronounced cooling of deep water in the Canterbury Basin, which is accompanied by equivalent cooling of surface waters in the Hampden section but less pronounced cooling at mid-Waipara. Overall cooling in Canterbury Basin during the middle Eocene resulted in a return to temperate conditions by ~42 Ma, perhaps earlier in the southern part of the basin (Fig. 6). Significantly warmer conditions are indicated for the East Tasman Plateau through the middle Eocene. Based on benthic foraminiferal $\delta^{18}O$ and Mg/Ca, BWT in the outermost shelf-upper bathyal part of Canterbury Basin reached 17–19 °C during the EECO, falling to 12–13 °C in the middle Eocene.

Our evidence for warm subtropical-cool tropical conditions in the southwest Pacific during the EECO agrees with paleontological evidence for the presence of a biota with tropical affinities (Hornibrook and deB, 1992), including foraminifera (Jenkins, 1968; Adams et al., 1990), coral (Adams et al., 1990), molluscs (Beu and Maxwell, 1990), mangroves and palms (Adams et al., 1990; Pocknall, 1990; Crouch and Visscher, 2003), during times of peak warmth in the Eocene.

5.5. Proxy-model comparison

Even when TEX_{86}^{L} is used to derive SSTs for the southwest Pacific, thermal gradients remain extremely low for the EECO (Fig. 2; ~5 °C over 65° of latitude). Such low gradients have proven difficult to produce in previous climate model simulations (Barron, 1987; Huber and Sloan, 2001). Here we compare proxy-based SSTs with modeled SSTs derived from two Eocene coupled climate model simulations based on lower and higher CO_2 concentrations (2240 and 4480 ppmv CO_2-equivalent; Fig. 7). The high greenhouse gas radiative forcing used in these simulations can be thought of as either representing a mix of greenhouse gases that were likely higher in the past (CO_2, CH_4, N_2O) or alternatively a crude means to account for the low sensitivity (~2 °C per doubling of CO_2) of the NCAR CCSM3 model. As has recently been shown (Lunt et al., 2012), all of the current generation of models produce qualitatively similar results once variations in their individual model sensitivity are taken into account. Although the lower estimates for SST, derived from the TEX_{86}^{L} proxy, are still significantly warmer than modeled mean annual SST for the southwest Pacific (Fig. 7A and B), proxy SSTs compare well with modeled SSTs for Austral summer (Fig. 7C and D), with particularly good agreement offshore eastern New Zealand (assuming the EECO median SST of 28 °C at Hampden is due to its shelf setting). Both low and high CO_2 models support the notion that deep sea temperatures in the middle Eocene and EECO record winter deep-water formation at the Antarctic margin (Fig. 7E and F).

A seasonal bias in SST proxies may be expected in high-latitude regions where seasonal temperature variations are at their most extreme. A summer bias in TEX_{86}-based SSTs for the Arctic Paleogene has previously been suggested (Sluijs et al. 2006, 2009) and is supported by terrestrial temperature indicators (Eberle et al., 2010). Given the differences in ecology and geochemical assumptions that underlie the three SST proxies considered here, a summer peak in archaeal consumption and

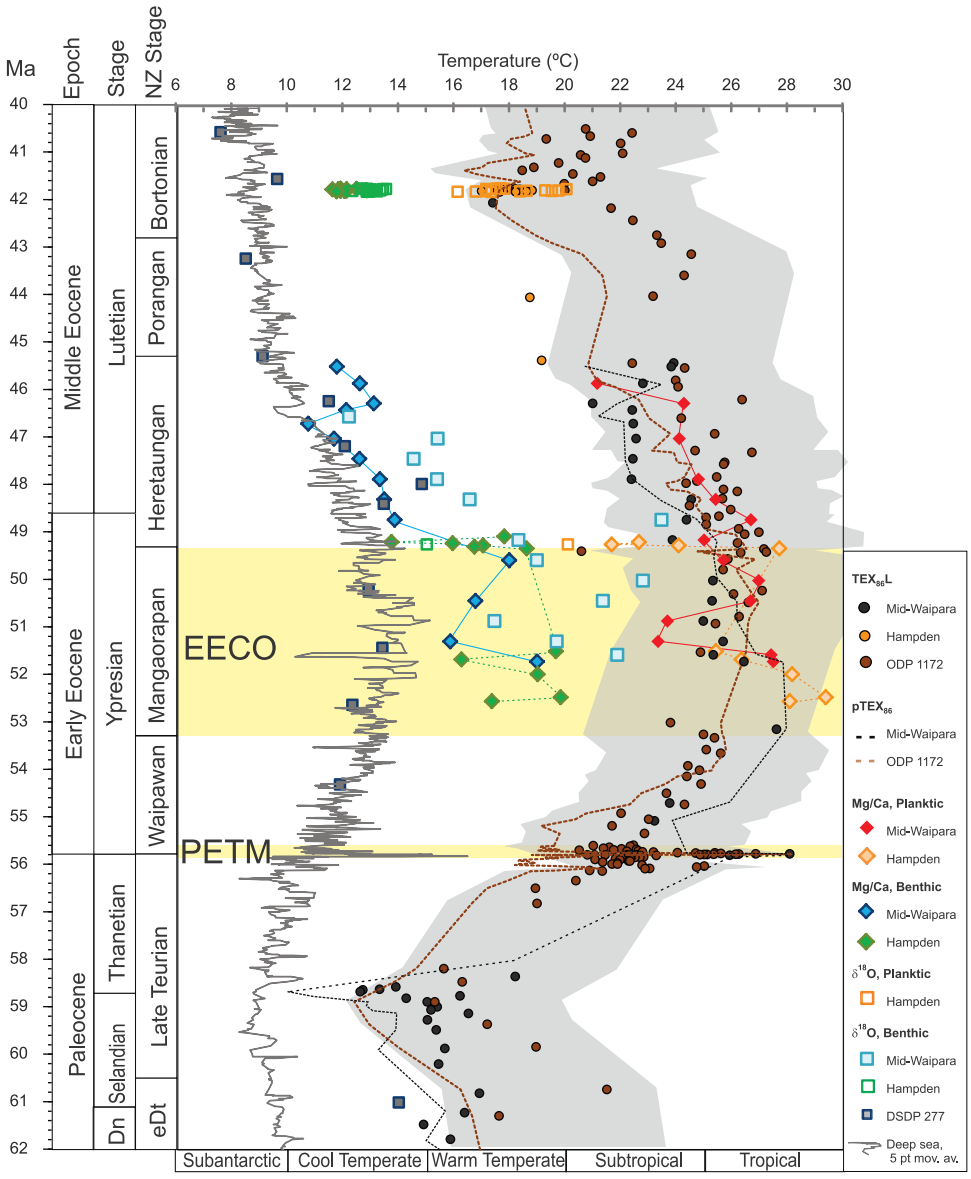

Fig. 6. Middle Paleocene to middle Eocene marine temperatures for the southwest Pacific estimated from TEX^{L}_{86}, $pTEX_{86}$, Mg/Ca and $\delta^{18}O$, with unreliable $\delta^{18}O$ data from mid-Waipara and DSDP Site 277 omitted. The gray shaded interval represents calibration error of ± 4 °C for TEX^{L}_{86}-based SSTs from ODP Site 1172 data series. Data sources: Burgess et al. (2008), Bijl et al. (2009), Cramer et al. (2009), Creech et al. (2010), Hollis et al. (2009), Shackleton and Kennett (1975), and Sluijs et al. (2011).

Table 1
Median temperature estimates for southwest Pacific sites and the deep sea over nine Paleocene–Eocene time slices. Additional data sources: DSDP 277 (Shackleton and Kennett, 1975), Deep sea (Cramer et al., 2009), MAAT (NZ: Kennedy, 2003; Huber and Caballero, 2011; Aus: Greenwood et al., 2003, 2004; Carpenter et al., 2012). Bold = warmest regional value, italics = coolest regional value.

	SST				BWT				MAAT	
Time interval	277	1172	HD	MW	Deep sea	277	HD	MW	NZ	Aus
MM Eocene (43–40 Ma)	10?	**21**	17	17	9	9	**12**	?		
EM Eocene (49–42 Ma)	13?	**25**	23	23	10	13	**17**	13		
EECO (53.3–49.3 Ma)	18?	26	**28**	26	13	13	**19**	17		
EE Eocene (55.5–53 Ma)	16?	23	?	23	12	12			20	22
PETM (55.8–55.6 Ma)	?	25	?	**27**	16	?	Na	?		
LL Paleocene (58.2–55.9 Ma)	?	**22**	?	*18*	10	?	Na	Na		
M/L Paleocene (58.8–58.3 Ma)	?	**16**	?	*13*	9	?	Na	Na		
M Paleocene (62–58.9 Ma)	17?	**19**	?	16	10	14	Na	?	11	

export would need to be coupled with summer calcification of planktic foraminiferal tests. Studies of productivity and ocean flux in the Australasian region support this inference. The flux of particulate organic matter is greatest in mid- to late-spring offshore eastern New Zealand (Nodder and Northcote, 2001) and production of surface-dwelling planktic foraminiferal production

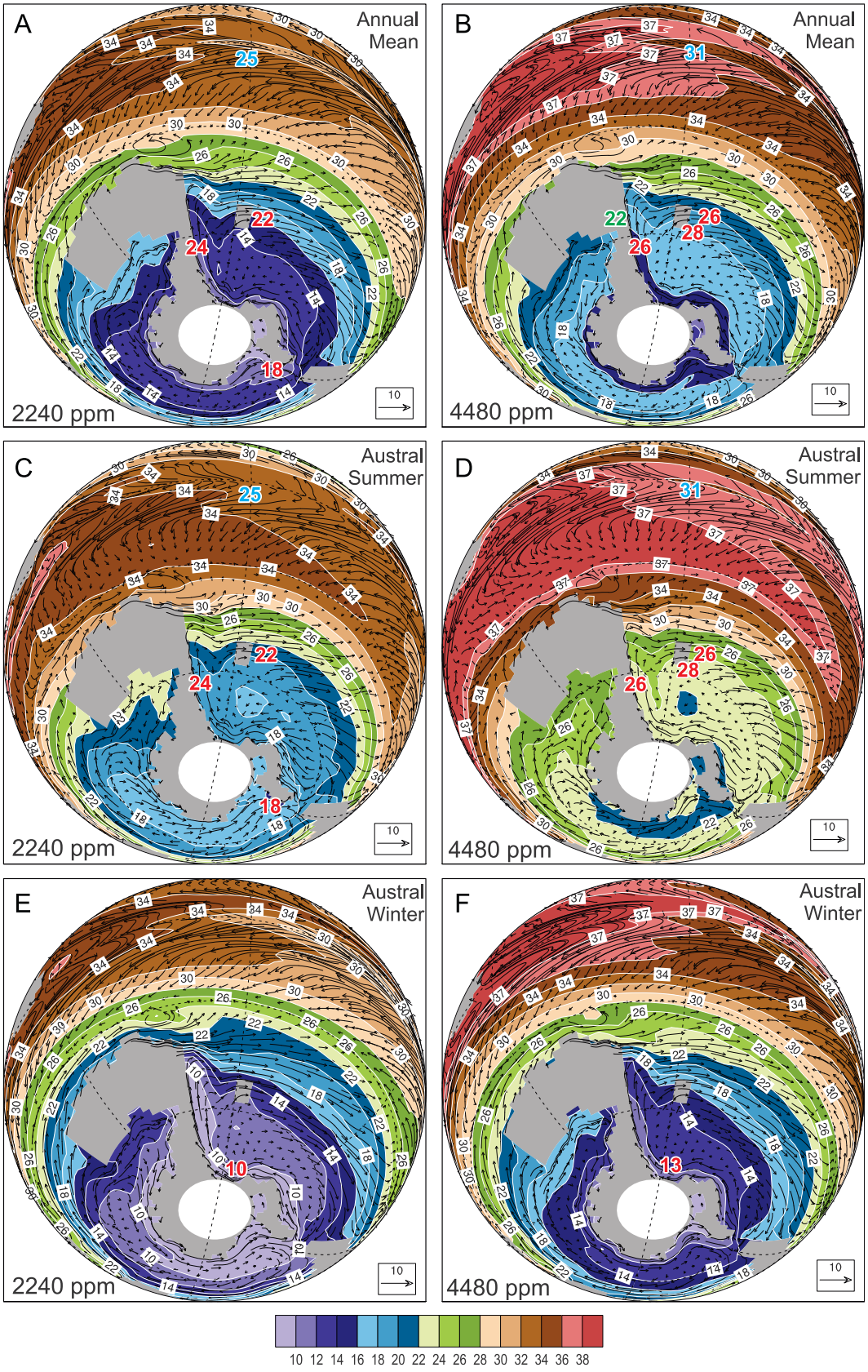

Fig. 7. Comparison of proxy SSTs for the middle Eocene (A, C, E) and EECO (B, D, F) with modeled Eocene SSTs for mean annual (A, B), Austral summer (C, D) and Austral winter (E, F) conditions under lower (A, C, E) and higher (B, D, F) degrees of greenhouse-gas forcing (2240 and 4480 ppmv CO_2-equivalent). Proxy SSTs (red & blue numbers) and MAAT (green number) are median values (see Table 1 and Supplemental files). Note that the Seymour Island record is now thought to be no older than early middle Eocene (Douglas et al., 2011). (For interpretation of the references to color in this figure legend, the reader is referred to the web version of this article.)

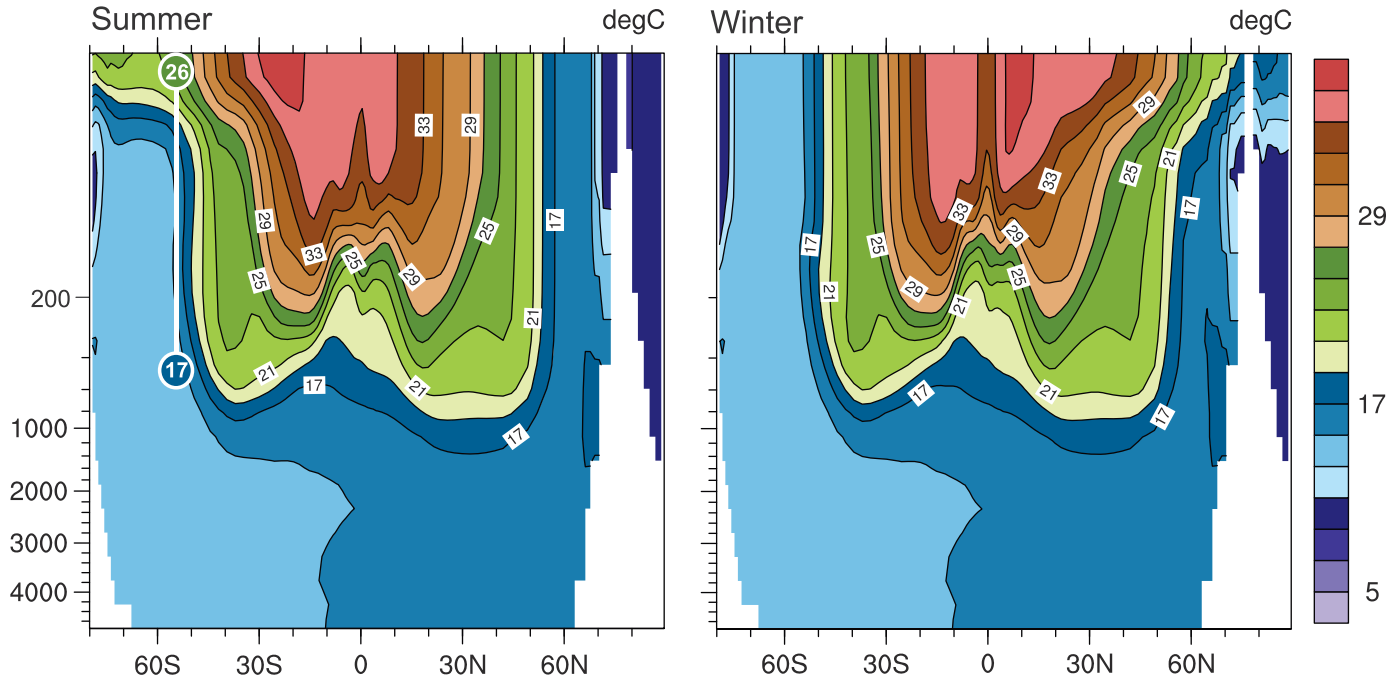

Fig. 8. Comparison of median proxy SST and BWT for the EECO at mid-Waipara with modeled, zonally averaged, temperature variation by water depth and latitude for Austral summer and Austral winter (4480 ppmv CO_2-equivalent) at 180° paleolongitude.

peaks in late spring or summer in the Southern Ocean (King and Howard, 2005).

The vertical temperature profile generated from our high CO_2 simulation shows pronounced seasonal changes in watermass structure south of 50°S (Fig. 8). For mid-Waipara, the proxy-derived SST–BWT gradient from 26 to 17 °C during the EECO is a very close match to the modeled vertical profile for summer at 55°S. A summer bias also explains two apparent mismatches in proxy temperatures that were highlighted in the introduction (Fig. 2): deep sea and local land temperatures. Deep-sea BWT is inferred to represent SST at high-latitude sites of deep water production, which primarily occurs during winter when the densest water is formed. A median BWT of 13 °C for the EECO (Table 1) agrees with modeled winter SST at ~80°S in the high CO_2 simulation (Figs. 7F and 8). Studies of leaf fossil assemblages from southeast Australia (60–65°S) indicated a mean annual air temperature (MAAT) at sea level of ~22 °C for the early Eocene (Greenwood et al., 2003, 2004; Carpenter et al., 2012) (Fig. 7B).

It has been argued that the current generation of climate models are failing to capture fundamental components of the greenhouse climate system that serve to amplify high-latitude temperature changes (Barron, 1987; Huber and Sloan, 1999, 2001; Huber, 2008; Valdes, 2011). If the southwest Pacific SSTs produced in this and earlier studies are indeed annual mean values then this interpretation may be correct. Models may have either overly weak radiative–convective (Abbot et al., 2009) or meridional heat transport feedbacks (Barron, 1987; Huber and Sloan, 2001). One area of active research is the role of ocean heat transport. For example, it is possible that warmer proxy SSTs for the western Tasman Sea (Fig. 7) may signal the influence of a proto-East Australian Current (EAC). The modern EAC delivers warm subtropical water to the southeast margin of Australia and to eastern New Zealand (Ridgway and Hill, 2009). A present-day warming trend has been linked to wind forcing associated with intensification of the subtropical gyre (Hill et al., 2008). A recent modeling study (Sijp et al., 2011) supports paleontological evidence (Kennett and Exon, 2004) indicating that, prior to the deepening of the Tasmanian Gateway during the Eocene–Oligocene transition, a proto-EAC may have delivered tropical to warm subtropical water into the South Tasman Sea and New Zealand region. The influence of this current may have intensified during times of extreme global warmth, such as the PETM and EECO. This current is capable of accounting for 2–4 °C (Sijp et al., 2011) of the SST offset.

Whilst early Eocene SST records for the southwest Pacific and Antarctic margin (Bijl et al., 2011) are considered anomalously warm by some authors (Keating-Bitonti et al., 2011; Pagani et al., 2011), it is worth noting that they may be the only reliable SST records for this time interval in the Southern Ocean. The Seymour Island SST record is now thought to be no older than middle Eocene (Houben, pers. comm., 2010) and the Eocene $\delta^{18}O$ values from planktic foraminifera at DSDP Site 277 and ODP Sites 690 and 738 appear to be variably affected by seafloor diagenesis (see Supplemental files).

6. Conclusions

Our analysis has taken a conservative approach to estimating SSTs in the southwest Pacific, which has included consideration of the assumptions that underlie temperature-proxy calibrations and temperature equations. We have developed a preliminary paleo-calibration for TEX_{86} that is based on multiproxy Eocene records from four sites representing a SST range of 15–34 °C. This paleo-calibration indicates that TEX_{86}^{L} is currently the most accurate TEX_{86}-based SST proxy for the southwest Pacific Paleogene and that previously cited SSTs may have been overestimated by 5–9 °C. The TEX_{86}^{L} proxy indicates that SST was typically in the range of 25–26 °C in the southwest Tasman Sea and Canterbury Basin during the PETM and EECO. SSTs derived from Mg/Ca for the EECO are consistent with TEX_{86}^{L} but indicate warmer SSTs in the shallower setting at Hampden.

The EECO broadly corresponds with the Mangaorapan stage (53.3–49.3 Ma) in the southwest Pacific, which is consistent with the stage recording an influx of plants and animals with tropical affinities (Hornibrook and deB, 1992). The base of the EECO is not

yet well-constrained locally but the warmest SSTs and BWTs are recorded in the lowest Mangaorapan samples from Canterbury Basin (Fig. 6). The termination of the EECO is very well delineated in Canterbury Basin by pronounced cooling of BWT at mid-Waipara and of both SST and BWT at Hampden. The duration of the EECO is less clear at ODP Site 1172. The nature and timing of onset is uncertain due to a lower Mangaorapan (~53–52 Ma) hiatus and the termination appears to occur gradually in the lower Heretaungan (~49 Ma). These differences may reflect the increasingly restricted influence of proto-EAC in the southwest Pacific during the Eocene, perhaps becoming more confined to the western Tasman Sea.

All Paleogene southwest Pacific SST proxies appear to suffer from a warm bias. Both low and high CO_2 models indicate a seasonal SST range of 10 °C, with winter polar SSTs in good agreement with benthic foraminifer $\delta^{18}O$ values for the middle and early Eocene (Fig. 7). The models are also consistent with what is known for land temperatures, with paleofloral data suggesting a MAAT of ~22° for southeast Australia during the EECO. Median SST estimates of 22–24 °C or 26–28 °C for the middle Eocene and EECO, respectively, can be reconciled with the models if they are biased towards summer temperatures and are influenced by the southward expansion of a warm proto-EAC. The final caveat in this exercise in reconciliation is to note that our EECO climate simulation is based on extraordinarily high CO_2 levels. Further work is needed to identify model improvements that will generate greater polar amplification of temperature at more tenable levels of atmospheric CO_2.

Acknowledgments

We thank Peter Barrett, Alan Beu, Peter Bijl, Giuseppe Cortese, Ben Cramer, Peter Douglas, Tom Dunkley-Jones, Sander Houben, Cam Nelson, Stefan Schouten, Dann Vanhove who contributed helpful comments, information and/or datasets. The study was supported by the GNS Global Change through Time Program and the New Zealand Marsden Fund. KT and LH acknowledge the UK NERC for support of their studentships, and RDP acknowledges the Royal Society Wolfson Research Merit Award. Huber was funded by the NSF Grant 0927946-ATM. This is PCCRC contribution number 11XX.

Appendix A. Supplementary material

Supplementary data associated with this article can be found in the online version at http://dx.doi.org/10.1016/j.epsl.2012.06.024.

References

Abbot, D.S., Huber, M., Bousquet, G., Walker, C.C. 2009. High-CO_2 cloud radiative forcing feedback over both land and ocean in a global climate model. Geophys. Res. Lett. 36, L05 702. http://dx.doi.org/10.1029/2008GL036703.

Adams, C.G., Lee, D.E., Rosen, B.R., 1990. Conflicting isotopic and biotic evidence for tropical sea-surface temperatures during the Tertiary. Palaeogeogr. Palaeoclimatol. Palaeoecol. 77, 289–313.

Anand, P., Elderfield, H., Conte, M.H., 2003. Calibration of Mg/Ca thermometry in planktonic foraminifera from a sediment trap time series. Paleoceanography 18 (2), 1050.

Barron, E., 1987. Eocene equator-to-pole surface ocean temperatures: a significant climate problem? Paleoceanography 2, 729–739.

Beerling, D.J., Royer, D.L., 2011. Convergent cenozoic CO_2 history. Nat. Geosci. 4, 418–420.

Bemis, B.E., Spero, H.J., Bijma, J., Lea, D.W., 1998. Reevaluation of the oxygen isotopic composition of planktonic foraminifera: experimental results and revised paleotemperature equations. Paleoceanography 13, 150–160.

Bertler, N.A.N., Barrett, P.J., 2010. Vanishing polar ice sheets. In: Dodson, J. (Ed.), Changing Climates, Earth Systems and Society, International Year of Planet Earth. Springer, Science+Business Media BV, pp. 49–83.

Beu, A.G., Maxwell, P.A., 1990. Cenozoic Mollusca of New Zealand. N. Z. Geol. Surv. Paleontol. Bull. 58, 518, pp.

Bice, K.L., Scotese, C.R., Seidov, D., Barron, E.J., 2000. Quantifying the role of geographic change in Cenozoic ocean heat transport using uncoupled atmosphere and ocean models. Palaeogeogr. Palaeoclimatol. Palaeoecol. 161 (3–4), 295–310.

Bijl, P.K., Schouten, S., Sluijs, A., Reichart, G.-J., Zachos, J.C., Brinkhuis, H., 2009. Early palaeogene temperature evolution of the southwest Pacific Ocean. Nature 461, 776–779.

Bijl, P.K., Houben, A.J.P., Schouten, S., Bohaty, S.M., Sluijs, A., Reichart, G.-J., Sinninghe Damste, J.S., Brinkhuis, H., 2010. Transient middle Eocene atmospheric CO_2 and temperature variations. Science 330, 819–821.

Bijl, P.K., Bendle, J., Pross, J., Schouten, S., Roehl, U., Stickley, C.E., Olney, M.L.T., L., T., Bohaty, S.M., Brinkhuis, H., Escutia, C., Scientists, E., 2011. Integrated stratigraphy of the Eocene Wilkes Land Margin, Antarctica; preliminary results from IODP Expedition 318: dinoflagellate cysts and TEX_{86} results. In: Egger, H. (Ed.), Climate and Biota of the Early Paleogene (CBEP 2011). Geologische Bundesanstalt, Salzburg, Austria, pp. 40.

Boersma, A., Premoli-Silva, I., Shackleton, N.J., 1987. Atlantic Eocene planktonic foraminiferal paleohydrographic indicators and stable isotope paleoceanography. Paleoceanography 2 (3), 287–331.

Broecker, W., Yu, J., 2011. What do we know about the evolution of Mg to Ca ratios in seawater? Paleoceanography 26, PA3203.

Burgess, C.E., Pearson, P.N., Lear, C.H., Morgans, H.E.G., Handley, L., Pancost, R.D., Schouten, S., 2008. Middle Eocene climate cyclicity in the southern Pacific: implications for global ice volume. Geology 36, 651–654.

Cande, S.C., Stock, J.M., 2004. Cenozoic reconstructions of the Australia–New Zealand–South Pacific sector of Antarctica. In: Exon, N., Kennett, J.P., Malone, M. (Eds.), The Cenozoic Southern Ocean. AGU Geophysical Monograph, Washington DC, USA, pp. 5–18.

Carpenter, R.J., Jordan, G.J., Macphail, M.K., Hill, R.S., 2012. Near-tropical early Eocene terrestrial temperatures at the Australo-Antarctic margin, western Tasmania. Geology 40, 267–270.

Coggon, R.M., Teagle, D.A.H., Smith-Duque, C.E., Alt, J.C., Cooper, M.J., 2010. Reconstructing past seawater Mg/Ca and Sr/Ca from mid-Ocean ridge flank calcium carbonate veins. Science 327, 1114–1117.

Coggon, R.M., Teagle, D.A.H., Dunkley Jones, T., 2011. Comment: what do we know about the evolution of Mg to Ca ratios in seawater? by Wally Broecker and Jimin Yu. Paleoceanography 26, PA3224.

Cooper, R.A. (Ed.), The New Zealand Geological Timescale. Institute of Geological and Nuclear Sciences Monograph, vol. 22. Institute of Geological and Nuclear Sciences, Lower Hutt (284 pp.).

Cramer, B.S., Toggweiler, J.R., Wright, J.D., Katz, M.E., Miller, K.G., 2009. Ocean overturning since the Late Cretaceous: inferences from a new benthic foraminiferal isotope compilation. Paleoceanography 24, PA4216.

Cramer, B.S., Miller, K.G., Barrett, P.J., Wright, J.D., 2011. Late Cretaceous–Neogene trends in deep ocean temperature and continental ice volume: reconciling records of benthic foraminiferal geochemistry ($\delta^{18}O$ and Mg/Ca) with sea level history. J. Geophys. Res.—Oceans 116, C12023.

Creech, J.B., Baker, J.A., Hollis, C.J., Morgans, H.E.G., Smith, E.G.C., 2010. Eocene sea temperatures for the mid-latitude southwest Pacific from Mg/Ca ratios in planktonic and benthic foraminifera. Earth Planet. Sci. Lett. 299 (3/4), 483–495, http://dx.doi.org/10.1016/j.epsl.2010.09.039.

Crouch, E.M., et al., 2001. Global dinoflagellate event associated with the late Paleocene thermal maximum. Geology 29 (4), 315–318.

Crouch, E.M., Brinkhuis, H., 2005. Environmental change across the Paleocene–Eocene transition from eastern New Zealand: a marine palynological approach. Mar. Micropaleontol. 56 (3/4), 138–160.

Crouch, E.M., Visscher, H., 2003. Terrestrial vegetation record across the initial Eocene thermal maximum at the Tawanui marine section, New Zealand. Spec. Pap./Geol. Soc. Am. 369, 351–363.

Douglas, P., Ivany, L.C., Keating-Bitonti, C.R., Pagani, M., Affek, H.P., 2011. Eocene sea surface temperature reconstructions from bivalve clumped isotope measurements. In: Egger, H. (Ed.), CBEP 2011. Geologische Bundesanstalt, pp. 66.

Eberle, J.J., Fricke, H.C., Humphrey, J.D., Hackett, L., Newbrey, M.G., Hutchison, J.H., 2010. Seasonal variability in Arctic temperatures during early Eocene time. Earth Planet. Sci. Lett. 296, 481–486.

Erez, J., Luz, B., 1983. Experimental paleotemperature equation for planktonic foraminifera. Geochim. Cosmochim. Acta 47, 1025–1031.

Farkaš, J., Böhm, F., Wallmann, K., Blenkinsop, J., Eisenhauer, A., van Geldern, R., Munnecke, A., Voigt, S., Veizer, J., 2007. Calcium isotope record of Phanerozoic oceans: implications for chemical evolution of seawater and its causative mechanisms. Geochim. Cosmochim. Acta 71, 5117–5134.

Gliozzi, A., Paoli, G., De Rosa, M., Gambacorta, A., 1983. Effect of isoprenoid cyclization on the transition temperature of lipids in thermophilic archaebacteria. Biochim. Biophys. Acta 735, 234–242.

Gradstein, F.M., Ogg, J.G., Smith, A.G. (Eds.), 2004. A Geological Time Scale 2004. Cambridge University Press, Cambridge, UK.

Greenwood, D., Moss, P., Rowett, A., Vadala, A., Keefe, R., 2003. Plant communities and climate, change in southeastern Australia during the early Paleogene. In: Wing, S.L., Gingerich, P.D., Schmitz, B., Thomas, E. (Ed.), Causes and consequences of globally warm climates in the early Paleogene. Geological Society of America special paper 369, pp. 365–380.

Greenwood, D.R., Wilf, P., Wing, S.L., Christophel, D.C., 2004. Paleotemperature estimation using Leaf-Margin Analysis: is Australia different? Palaios 19, 129–142.
Handley, L., Crouch, E.M., Pancost, R.D., 2011. A New Zealand record of sea level rise and environmental change during the Paleocene–Eocene thermal maximum. Palaeogeogr. Palaeoclimatol. Palaeoecol. 305 (1-4), 185–200.
Hansen, J., Sato, M., Kharecha, P., Beerling, D.J., Berner, R., Masson-Delmotte, V., Pagani, M., Raymo, M., Royer, D.L., Zachos, J.C., 2008. Target atmospheric CO_2: where should humanity aim? Open Atmos. Sci. J. 2, 217–231.
Hasiuk, F.J., Lohmann, K.C., 2010. Application of calcite Mg partitioning functions to the reconstruction of paleocean Mg/Ca. Geochim. Cosmochim. Acta 74, 6751–6763.
Hill, K.L., Rintoul, S.R., Coleman, R., Ridgway, K.R., 2008. Wind forced low frequency variability of the East Australia current. Geophys. Res. Lett. 35, L08602.
Ho, S.L., Yamamoto, M., Mollenhauer, G., Minagawa, M., 2011. Core top TEX86 values in the south and equatorial Pacific. Org. Geochem. 42, 94–99.
Hollis, C.J., Strong, C.P., Rodgers, K.A., Rogers, K.M., 2003. Paleoenvironmental changes across the cretaceous/tertiary boundary at Flaxbourne River and Woodside Creek, Eastern Marlborough, New Zealand. N. Z. J. Geol. Geophys. 46, 177–197.
Hollis, C.J., Dickens, G.R., Field, B.D., Jones, C.J., Strong, C.P., 2005. The Paleocene–Eocene transition at Mead Stream, New Zealand: a southern Pacific record of early Cenozoic global change. Palaeogeogr. Palaeoclimatol. Palaeoecol. 215, 313–343.
Hollis, C.J., Handley, L., Crouch, E.M., Morgans, H.E.G., Baker, J.A., Creech, J., Collins, K.S., Gibbs, S.J., Huber, M., Schouten, S., Zachos, J.C., Pancost, R.D., 2009. Tropical sea temperatures in the high-latitude South Pacific. Geology 37, 99–102.
Hollis, C.J., et al., 2010. Calibration of the New Zealand Cretaceous-Cenozoic Timescale to GTS2004. GNS Science Report, 2010/43, 20 pp.
Hopmans, E.C., Weijers, J.W.H., Schefuß, E., Hertford, L., Sinninghe Damsté, J.S., Schouten, S., 2004. A novel proxy for terrestrial organic matter in sediments based on branched and isoprenoid tetraether lipids. Earth Planet. Sci. Lett. 224, 107–116.
Hornibrook, N., deB., 1992. New Zealand Cenozoic marine paleoclimates: a review based on the distribution of some shallow water and terrestrial biota. In: Tsuchi, R., Ingle, J.C. (Eds.), Pacific Neogene: Environment, Evolution and Events. University of Tokyo Press, Tokyo, pp. 83–106.
Huber, M., 2008. A hotter greenhouse? Science 321, 353–354.
Huber, M., Caballero, R., 2011. The early Eocene equable climate problem revisited. Clim. Past Discuss. 7, 241–304.
Huber, M., Sloan, L.C., 1999. Warm climate transitions: a general circulation modeling study of the late Paleocene thermal maximum (approximately 56 Ma). J. Geophys. Res. D Atmos. 104 (14), 16,633–16,655.
Huber, M., Sloan, L.C., 2001. Heat transport, deep waters, and thermal gradients: coupled simulation of an Eocene greenhouse climate. Geophys. Res. Lett. 28 (18), 3481–3484.
Huber, M., Sloan, L.C., Shellito, C., 2003. Early Paleogene oceans and climate: fully coupled modeling approach using the NCAR CCSM. In: Wing, S.L., Gingerich, P.D., Schmitz, B., Thomas, E. (Eds.), Causes and Consequences of Globally Warm Climates in the Early Paleogene. Geological Society of America, pp. 25–47 (Special Paper 369).
Huguet, C., Schimmelmann, A., Thunell, R., Lourens, L.J., Sinninghe Damsté, J.S., Schouten, S., 2007. A study of the TEX86 paleothermometer in the water column and sediments of the Santa Barbara Basin, California. Paleoceanography 22, PA3203.
Ivany, L.C., Lohmann, K.C., Hasiuk, F., Blake, D.B., Glass, A., Aronson, R.B., Moody, R.M., 2008. Eocene climate record of a high southern latitude continental shelf: Seymour Island, Antarctica. GSA Bull. 120, 659–678.
Jenkins, D.G., 1968. Planktonic foraminiferida as indicators of New Zealand Tertiary paleotemperatures. Tuatara 16, 32–37.
Keating-Bitonti, C.R., Ivany, L.C., Affek, H.P., Douglas, P., Samson, S.D., 2011. Warm, not super-hot, temperatures in the early Eocene subtropics. Geology 39, 771–774.
Kennedy, E.M., 2003. Late Cretaceous and Paleocene terrestrial climates of New Zealand: leaf fossil evidence from South Island assemblages. N. Z. J. Geol. Geophys. 46, 295–306.
Kennett, J.P., Exon, N.F., 2004. Paleoceanographic evolution of the Tasmanian Seaway and its climatic implications. In: Exon, N.F., Kennett, J.P., Malone, M.J. (Eds.), The Cenozoic Southern Ocean: Tectonics, Sedimentation, and Climate Change between Australia and Antarctica. AGU, Washington, DC, pp. 345–367.
Kiehl, J., 2010. Lessons from Earth's past. Science 331, 158–159.
Killops, S.D., Hollis, C.J., Morgans, H.E.G., Sutherland, R., Field, B.D., Leckie, D.A., 2000. Paleoceanographic significance of Late Paleocene dysaerobia at the shelf/slope break around New Zealand. Palaeogeogr. Palaeoclimatol. Palaeoecol. 156, 51–70.
Kim, J.-H., Schouten, S., Hopmans, E.C., Donner, B., Sinninghe Damste, J.S., 2008. Global sediment core-top calibration of the TEX_{86} paleothermometer in the ocean. Geochim. Cosmochim. Acta 72, 1154–1173.
Kim, J.-H., Meer, J.V.D., Schouten, S., Helmke, P., Willmott, V., Sangiorgi, F., Koç, N., Hopmans, E.C., Sinninghe Damsté, J.S., 2010. New indices and calibrations derived from the distribution of crenarchaeal isoprenoid tetraether lipids: implications for past sea surface temperature reconstructions. Geochim. Cosmochim. Acta 74 (16), 4639–4654.
Kim, S.-T., O'Neil, J.R., 1997. Equilibrium and nonequilibrium oxygen isotope effects in synthetic carbonates. Geochim. Cosmochim. Acta 61, 3461–3475.
King, A.L., Howard, W.R., 2005. $\delta^{18}O$ seasonality of planktonic foraminifera from Southern Ocean sediment traps: latitudinal gradients and implications for paleoclimate reconstructions. Mar. Micropaleontol. 56, 1–24.
King, P.R., Naish, T.R., Browne, G.H., Field, B.D., Edbrooke, S.W., 1999. Cretaceous to Recent Sedimentary Patterns in New Zealand, 1. Institute of Geological and Nuclear Sciences Folio Series (35 pp.).
Kozdon, R., Kelly, D.C., Kita, N.T., Fournelle, J.H., Valley, J.W., 2011. Planktonic foraminiferal oxygen isotope analysis by ion microprobe technique suggests warm tropical sea surface temperatures during the Early Paleogene. Paleoceanography 26, PA3206.
Kurtz, A.C., Kump, L.R., Arthur, M.A., Zachos, J.C., Paytan, A., 2003. Early Cenozoic decoupling of the global carbon and sulfur cycles. Paleoceanography 18, 1090, http://dx.doi.org/10.1029/2003PA000908.
Lear, C.H., Elderfield, H., Wilson, P.A., 2000. Cenozoic deep-sea temperatures and global ice volumes from Mg/Ca in benthic foraminiferal calcite. Science 287, 269–272.
Lear, C.H., Rosenthal, Y., Slowey, N., 2002. Benthic foraminiferal Mg/Ca-paleothermometry: a revised core-top calibration. Geochim. Cosmochim. Acta 66, 3375–3387.
Lear, C.H., Mawbey, E.M., Rosenthal, Y., 2010. Cenozoic benthic foraminiferal Mg/Ca and Li/Ca records: toward unlocking temperatures and saturation states. Paleoceanography 25, 4215, http://dx.doi.org/10.1029/2009pa001880.
Liu, Z., Pagani, M., Zinniker, D., DeConto, R., Huber, M., Brinkhuis, H., Shah, S.R., Leckie, R.M., Pearson, A., 2009. Global cooling during the Eocene–Oligocene climate transition. Science 323, 1187–1190.
Lunt, D.J., Dunkley Jones, T., Heinemann, M., Huber, M., LeGrande, A., Winguth, A., Loptson, C., Marotzke, J., Tindall, J., Valdes, P., Winguth, C., 2012. A model-data comparison for a multi-model ensemble of early Eocene atmosphere–ocean simulations: EoMIP. Clim. Past Discuss. 8, 1229–1273.
McInerney, F.A., Wing, S.L., 2011. The Paleocene–Eocene thermal maximum: a perturbation of carbon cycle, climate, and biosphere with implications for the future. Annu. Rev. Earth Planet. Sci. 39 (1), 489–516.
Morgans, H.E.G., 2009. Late Paleocene to middle Eocene foraminiferal biostratigraphy of the Hampden Beach section, eastern South Island, New Zealand. N. Z. J. Geol. Geophys. 52, 273–320.
Morgans, H.E.G., Jones, C.M., Crouch, E.M., Field, B.D., Hollis, C.J., Raine, J.I., Strong, C.P., Wilson, G.J., 2005. Upper Cretaceous to Eocene Stratigraphy and Sample Collections, Mid-Waipara River Section, North Canterbury. Institute of Geological and Nuclear Sciences Science Report 2003/08.
Nodder, S.D., Northcote, L.C., 2001. Episodic particulate fluxes at southern temperate mid-latitudes (42–45°S) in the Subtropical Front, east of New Zealand. Deep-Sea Res. Part I, Oceanogr. Res. Pap. 48 (3), 833–864.
Ogg, J.G., Ogg, G., Gradstein, F.M., 2008. The Concise Geologic Time Scale. Cambridge University Press, New York, USA.
Pagani, M., Huber, M., Liu, Z., Bohaty, S.M., Henderiks, J., Sijp, W., Krishnan, S., DeConto, R.M., 2011. The role of carbon dioxide during the onset of Antarctic glaciation. Science 334, 1261–1264.
Pearson, P.N., Palmer, M.R., 2000. Atmospheric carbon dioxide concentrations over the past 60 million years. Nature 406, 695–699.
Pearson, P.N., Olsson, R.K., Huber, B.T., Hemleben, C., Berggren, W.A., (Eds.), 2006. Atlas of Eocene Planktonic Foraminifera. Cushman Foundation Special Publication No. 41, 514 pp.
Pearson, P.N., van Dongen, B.E., Nicholas, C.J., Pancost, R.D., Schouten, S., Singano, J.M., Wade, B.S., 2007. Stable warm tropical climate through the Eocene Epoch. Geology 35, 211–214.
Pocknall, D.T., 1990. Palynological evidence for the early to middle Eocene vegetation and climate history of New Zealand. Rev. Palaeobot. Palynol. 65, 57–69.
Ridgway, K., Hill, K., 2009. The East Australian Current. In: Poloczanska, E.S., Hobday, A.J., Richardson, A.J. (Eds.), A Marine Climate Change Impacts and Adaptation Report Card for Australia 2009. NCCARF Publication 05/09.
Roberts, C.D., LeGrande, A.N., Tripati, A.K., 2011. Sensitivity of seawater oxygen isotopes to climatic and tectonic boundary conditions in an early Paleogene simulation with GISS ModelE-R. Paleoceanography 26, PA4203, http://dx.doi.org/10.1029/2010pa002025.
Schiøler, P., Rogers, K., Sykes, R., Hollis, C.J., Ilg, B., Meadows, D., Roncaglia, L., Uruski, C., 2010. Palynofacies, organic geochemistry and depositional environment of the Tartan Formation (Late Paleocene), a potential source rock in the Great South Basin, New Zealand. Mar. Pet. Geol. 27, 351–369.
Schouten, S., Hopmans, E.C., Schefu[ss], E., Sinninghe Damste, J.S., 2002. Distributional variations in marine crenarchaeotal membrane lipids: a new tool for reconstructing ancient sea water temperatures? Earth Planet. Sci. Lett. 204, 265–274.
Schouten, S., van der Meer, M.T.J., Hopmans, E.C., Rijpstra, W.I.C., Reysenbach, A.L., Ward, D.M., Damsté, J.S.S., 2007. Archael and bacterial glycerol dialkyl glycerol tetraether lipids in hot springs of Yellowstone National Park. Appl. Environ. Microbiol. 73, 6181–6191.
Sexton, P.F., Wilson, P.A., Pearson, P.N., 2006. Microstructural and geochemical perspectives on planktic foraminiferal preservation: "Glassy" versus "Frosty". Geochem. Geophys. Geosyst.—G3, 7, http://dx.doi.org/10.1029/2006GC001291.
Shackleton, N.J., 1974. Attainment of isotopic equilibrium between ocean water and the benthonic foraminifera genus *Uvigerina*: isotopic changes in the ocean during the last glacial. CNRS Colloq. Int. 219, 203–209.

Shackleton, N.J., Kennett, J.P., 1975. Paleotemperature History of the Cenozoic and the Initiation of Antarctic Glaciation: Oxygen and Carbon Isotope Analyses in DSDP Sites 277, 279, and 281. Initial Reports of the Deep Sea Drilling Project, vol. 29, pp. 743–755.

Sijp, W.P., England, M.H., Huber, M., 2011. Effect of the deepening of the Tasman Gateway on the global ocean. Paleoceanography 26, PA4207, http://dx.doi.org/10.1029/2011PA002143.

Sluijs, A., Schouten, S., Donders, T.H., Schoon, P.L., Rohl, U., Reichart, G.-J., Sangiorgi, F., Kim, J.-H., Sinninghe Damste, J.S., Brinkhuis, H., 2009. Warm and wet conditions in the Arctic region during Eocene thermal maximum 2. Nat. Geosci. 2, 777–780.

Sluijs, A., Schouten, S., Pagani, M., Woltering, M., Brinkhuis, H., Sinninghe Damste, J.S., Dickens, G.R., Huber, M., Reichart, G.-J., Stein, R., Matthiessen, J., Lourens, L.J., Pedentchouk, N., Backman, J., Moran, K., the Expedition Science Party, 2006. Subtropical Arctic Ocean temperatures during the Palaeocene/Eocene thermal maximum. Nature 441, 610–613.

Sluijs, A., Bijl, P.K., Schouten, S., Roehl, U., Reichart, G.J., Brinkhuis, H., 2011. Southern ocean warming, sea level and hydrological change during the Paleocene–Eocene thermal maximum. Clim. Past 7, 47–61.

Tindall, J., Flecker, R., Valdes, P., Schmidt, D.N., Markwick, P., Harris, J., 2010. Modeling the oxygen isotope distribution of ancient seawater using a coupled ocean-atmosphere GCM: implications for reconstructing early Eocene climate. Earth Planet. Sci. Lett. 292, 265–273.

Tripati, A.K., Delaney, M.L., Zachos, J.C., Anderson, L.D., Kelly, D.C., Harry, E., 2003. Tropical sea-surface temperature reconstruction for the early Paleogene using Mg/Ca ratios of planktonic foraminifera. Paleoceanography 18, 1101, http://dx.doi.org/10.1029/2003PA000937.

Valdes, P., 2011. Built for stability. Nat. Geosci. 4, 414–416.

Vanhove, D., Stassen, P., Speijer, R., Steurbalt, E., 2011. Assessing paleotemperature and seasonality during the early Eocene climatic optimum (EECO) in the Belgian Basin by means of fish otolith stable O and C isotopes. Geol. Belg. 14, 143–158.

Weijers, J.W.H., Schouten, S., Spaargaren, O.C., Sinninghe Damsté, J.S., 2006. Occurrence and distribution of tetraether membrane lipids in soils: implications for the use of TEX_{86} proxy and the BIT index. Org. Geochem. 37, 1680–1693.

Winguth, A., Shellito, C., Shields, C., Winguth, C., 2010. Climate Response at the Paleocene–Eocene thermal maximum to greenhouse gas forcing: a model study with CCSM3. J. Clim. 23, 2562–2584.

Wuchter, C., Schouten, S., Wakeham, S.G., Sinninghe Damsté, J.S., 2006. Archaeal tetraether membrane lipid fluxes in the northeastern Pacific and the Arabian Sea: implications for TEX_{86} paleothermometry. Paleoceanography 21 (4), PA4208.

Zachos, J.C., Arthur, M.A., 1986. Paleoceanography of the Cretaceous/tertiary boundary event; inferences from stable isotopic and other data. Paleoceanography 1 (1), 5–26.

Zachos, J.C., Stott, L.D., Lohmann, K.C., 1994. Evolution of early Cenozoic marine temperatures. Paleoceanography 9, 353–387.

Zachos, J.C., Schouten, S., Bohaty, S., Quattlebaum, T., Sluijs, A., Brinkhuis, H., Gibbs, S.J., Bralower, T.J., 2006. Extreme warming of mid-latitude coastal ocean during the Paleocene–Eocene thermal maximum: inferences from TEX_{86} and isotope data. Geology 34, 737–740.

Zachos, J.C., Dickens, G.R., Zeebe, R.E., 2008. An early Cenozoic perspective on greenhouse warming and carbon-cycle dynamics. Nature 451, 279–283.

Zachos, J.C., Pagani, M., Sloan, L.C., Thomas, E., Billups, K., 2001. Trends, rhythms, and aberrations in global climate 65 Ma to present. Science 292, 686–693.